Cite this article as: Cancado de Faria R., et al. (2023). STAT1 Drives the Interferon-Like Response and Aging Hallmarks in Progeria, *AgingBio*, *1*, 1–15. doi: 10.59368/agingbio.20230009.

Research Paper

STAT1 Drives the Interferon-Like Response and Aging Hallmarks in Progeria

Rafael Cancado de Faria,[1] Elena V. Shashkova,[1] Colin Flaveny,[2,3] Angel Baldan,[1] Kyle S. McCommis,[1] and Susana Gonzalo[1,*]

[1]Edward A. Doisy Department of Biochemistry and Molecular Biology, Saint Louis University School of Medicine, St. Louis, MO, USA
[2]Department of Pharmacology and Physiology, Saint Louis University School of Medicine, St. Louis, MO, USA
[3]Now at Pfizer Translation Sciences, Oncology Research Unit, San Diego, CA, USA
[*]Corresponding author: susana.gonzalohervas@health.slu.edu; sgonzalo@slu.edu
https://doi.org/10.59368/agingbio.20230009

Hutchinson–Gilford progeria syndrome (HGPS), a devastating premature aging disease caused by the mutant lamin-A protein "progerin," features robust sterile inflammation/interferon (IFN)-like response. Targeting inflammation delays cellular and organismal HGPS phenotypes. However, specific mechanisms driving the sterile inflammation/IFN-like response and how this response causes tissue degeneration/loss in HGPS are unknown. We demonstrate that signal transducer and activator of transcription 1 (STAT1) drives the IFN-like response and aging phenotypes in HGPS cellular and mouse models. Calcitriol and baricitinib strongly repress sterile inflammation/IFN-like response, improving hallmarks of progerin-expressing cells such as mitochondrial, autophagy, and proliferation defects. *In vivo*, calcitriol or baricitinib extend lifespan of progeria mice, and baricitinib alone or combined with a high-caloric/high-fat diet has a remarkable impact reducing skin, aortic, and adipose tissue degeneration. Critically, Stat1 haploinsufficiency reduces tissue degeneration/loss and extends lifespan of progeria mice, recapitulating baricitinib benefits. Our study unveils STAT1 as a driver of the IFN-like response and HGPS pathology and suggests that aberrant STAT1 signaling contributes to aging, providing new therapeutic possibilities for HGPS and other inflammation/IFN response-associated diseases.

Introduction

Inflammation is a hallmark of aging and age-related diseases[1]. Ideally, inflammation should resolve immediately after elimination of an insult to maintain tissue/organismal homeostasis. However, low-grade persistent inflammation occurs in most aged/prematurely aged individuals, contributing to the development of conditions, such as cancer, cardiovascular, and neurodegenerative diseases[2–6], as well as metabolic disorders, including sarcopenia, insulin resistance, lipodystrophy, and atherosclerosis[7–11].

Hutchinson–Gilford progeria syndrome (HGPS) is a rare and devastating premature aging disease that resembles many features of normal aging at cellular and organismal level, including inflammation[12]. Patients diagnosed with HGPS develop skin abnormalities, alopecia, loss of bone density, muscular dystrophy, and lipodystrophy[13–15]. HGPS patients commonly die in their teens from cardiovascular complications, and the only FDA (Food and Drug Administration Agency of the US Department of Health and Human Services)-approved therapy, a farnesyltransferase inhibitor (lonafarnib), provides limited benefits to HGPS patients[16], stressing the need for new therapeutic targets.

HGPS results from a *LMNA* gene mutation and expression of a truncated lamin A protein, progerin, which causes cellular toxicity[17,18]. Progerin induces changes in cellular metabolism, with anomalies in energy production and expenditure, like senescent cells[14,19]. There are reports of mitochondrial dysfunction[20–22], deficiencies in autophagy[23], and altered nutrient sensing pathways[24,25], which could underlie cellular metabolic problems. We found severe metabolic problems in $Lmna^{G609G/G609G}$ progeria mice, with features of starvation, cachexia, and lipodystrophy, which were significantly reduced by feeding mice fat-rich/high-caloric diets[15]. Yet the mechanisms underlying cellular and organismal metabolic problems are unknown.

In addition to metabolic changes, progerin causes alterations in nuclear architecture, telomere stability[26–28], and DNA replication and repair[29,30], eliciting replication stress and genomic instability. These are accompanied by leakage and buildup of self-DNA in the cytoplasm, which can trigger a "pathogen-free" antiviral/interferon (IFN) response[31]. Cytoplasmic DNA is recognized by pattern recognition receptors (PRRs) that signal the activation of TANK-binding kinase 1 (TBK1) and inhibitor of nuclear factor kappa B kinase (IKK) kinases via the adaptor protein Stimulator of Interferon Genes (STING). These kinases activate transcription factors IRF3 and NFkB, respectively, that induce the expression of IFNs and other inflammatory cytokines, which can trigger an IFN response through autocrine and paracrine signaling[32,33]. We previously found an upregulation of the antiviral/innate immune/IFN-like response pathway (herein referred to as IFN response), namely PRRs, STING, IFN-stimulated genes (ISGs), and signal transducer and activator of transcription 1 (STAT1) in HGPS patients-derived fibroblasts, and other progerin-expressing cell models[29,30]. Interestingly, calcitriol administration ameliorates

cellular progeria hallmarks[34], including DNA damage, replication stress, and sterile inflammation/IFN response[29,30]. Overall, these studies suggested that sterile inflammation/IFN response might underlie the severe metabolic and degenerative phenotypes of HGPS, as shown for other aging-related phenotypes[3,35,36]. To test this hypothesis and shed some light onto the molecular mechanisms linking the IFN response to aging, we defined the impact of targeting the IFN response in HGPS cellular and animal models.

There are data supporting that inflammation contributes to progeroid phenotypes. For instance, inhibition of NOD-, LRR- and pyrin domain-containing protein 3 (NLRP3) inflammasome or IL-6 signaling in cellular and mouse models of HGPS mitigates inflammation, delays the onset of progeroid phenotypes, and extends lifespan[36,37]. In addition, blocking Janus kinase (JAK)-STAT pathway signaling with ruxolitinib reduces cellular markers of senescence. *In vivo*, ruxolitinib alleviates rib fractures, bone mineral loss, and grip strength in *Zmpste24*$^{-/-}$ mice; a model of progeria characterized by expression of prelamin A[35]. Ruxolitinib treatment of *Zmpste24*$^{-/-}$ mice shows a trend toward increased survival. A ruxolitinib analog, baricitinib, also improves the health of progerin-expressing cells and reduces the cellular toxicity of lonafarnib[38,39]. However, the specific target/s of ruxolitinib and baricitinib responsible for the improvement of progeria phenotypes *in vitro* is/are not known. In addition, the impact of baricitinib treatment on mouse models of HGPS that express progerin (*Lmna*$^{G609G/G609G}$ mice) is not known. These JAK-STAT pathway inhibitors can block phosphorylation and activation of different STAT family members. In our previous studies, STAT1 knockdown in progerin-expressing cells reduced inflammation and cellular decline[29], pointing to STAT1 as a contributor to the progeroid phenotypes at least at a cellular level. However, the molecular mechanisms underlying STAT1 contribution to cellular decline and perhaps organismal deterioration are not known.

Here, we show that targeting sterile inflammation/IFN response offers significant benefits to progerin-expressing cells and HGPS mice (*Lmna*$^{G609G/G609G}$). Calcitriol, which inhibits the whole IFN response, shows new mechanisms of action, ameliorating progerin-induced metabolic alterations, including mitochondrial dysfunction and autophagy, and significantly improving longevity of progeria mice. Similarly, blocking of JAK-STAT-mediated sterile inflammation with baricitinib mitigates metabolic alterations and cellular decline in progerin-expressing fibroblasts. Critically, baricitinib alone, but especially in combination with high-fat/high-caloric diet, considerably extends lifespan and healthspan of progeria mice, and remarkably delays tissue degeneration phenotypes such as thinning of skin, loss of aortic smooth muscle cells (SMCs), and lipodystrophy. Importantly, we demonstrate that STAT1 is a key molecular driver of organismal decline and tissue wasting in progeria mice, and an important mediator of the therapeutic benefits exerted by baricitinib. Altogether, our data shed light on specific factors in the IFN response that are driving cellular decline, tissue degeneration, and overall organismal premature aging. Our findings also provide novel single and/or combinatorial therapeutic approaches to slow down premature aging in HGPS patients.

Results

Progerin triggers metabolic alterations and sterile inflammation/IFN response

Metabolic alterations have been reported in HGPS cells, such as alterations in nutrient sensing pathways[24,25,40], autophagy[23,39], and mitochondrial dysfunction[20–22,38]. However, the discrepant results reported have raised controversy about the molecular mechanisms involved and their relevance to HGPS pathology. To characterize these metabolic pathways in isogenic cells, we used a doxycycline (doxy)-inducible system for progerin expression in Human Dermal Fibroblasts (HDFs). Progerin expression for increasing periods of time (2–16 days) leads to activation (phosphorylation of threonie 172) of a master regulator of metabolism that controls energy balances, AMP-activated protein kinase (AMPK) (Fig. 1A,B). Active AMPK can reduce mTORC1 activity attenuating anabolic pathways and stimulating catabolism, such as autophagy. We find a modest reduction in mammalian target of rapamycin complex 1 (mTORC1) complex activity with a decrease in phosphorylation of its downstream targets, unc-51 like autophagy activating kinase 1 (ULK1) (serine 757), and S6 Ribosomal Protein (S6RP) (serines 240/244) (Fig. 1A, B). In addition, progerin-expressing cells show increased levels of the autophagosome marker LC3-II (LC3-phosphatidylethanolamine conjugate), and a reduction in the autophagy cargo receptor p62 (Fig. 1A,B). However, autophagy flux blockage with an autophagosome–lysosome fusion inhibitor, chloroquine, did not enhance LC3-II accumulation upon progerin expression, implying impaired autophagy flux (Fig. 1C,D). In addition, we observed metabolic reprogramming of glucose utilization toward increased glycolysis in cells expressing progerin, with increased lactate concentration in cell media compared to control cells (Fig. 1E). This is consistent with RNAseq data on HGPS fibroblasts showing higher levels of glycolysis-related transcripts compared to normal fibroblasts (**Fig. S1A**). Moreover, we find significantly reduced mitochondrial oxygen consumption rates (OCRs) measured by Seahorse (Fig. 1F and **Fig. S1B**). Specifically, progerin expression reduced basal, maximal, and ATP-linked respiration, as well as proton leak respiration. Overall, these results indicate a starvation phenotype in doxy-induced progerin-expressing cells mirroring those observed in senescent cells[19,41].

Along with alterations in nutrient sensing pathways and energy metabolism, progerin triggers sterile inflammation in HDFs. In previous studies, we found the upregulation of genes and activation of proteins involved in antiviral/IFN response in cells expressing progerin[29,30]. Here, we find activation of TBK1, a kinase that mediates the synthesis of inflammatory cytokines[42], and STAT1, a transcription factor involved in the expression of hundreds of ISGs, including interferon-stimulated gene 15 (ISG15) and retinoic acid-inducible gene I (RIG-I)[29,30] (Fig. 1G and **Fig. S1C**). Importantly, doxycycline treatment of either neonatal or adult primary HDFs, in the absence of inducible progerin expression, did not contribute to the activation of sterile inflammation, which indicates no involvement of doxycycline in the phenotype of progerin-expressing cells (**Fig. S1D**). Our results demonstrate that the robust activation of a sterile inflammation/IFN-like response in cells expressing progerin is concomitant with metabolic alterations such as dysfunctional mitochondrial respiration and reduced autophagy flux.

Reducing sterile inflammation with calcitriol improves metabolic function *in vitro* and extends lifespan of progeria mice

Interest is emerging about the cross-talk between antiviral/innate immunity response and metabolic alterations in different contexts[3,43–47]. To determine whether targeting sterile inflammation ameliorates energy metabolism and cellular health, we treated progerin-expressing cells with calcitriol, the hormonal

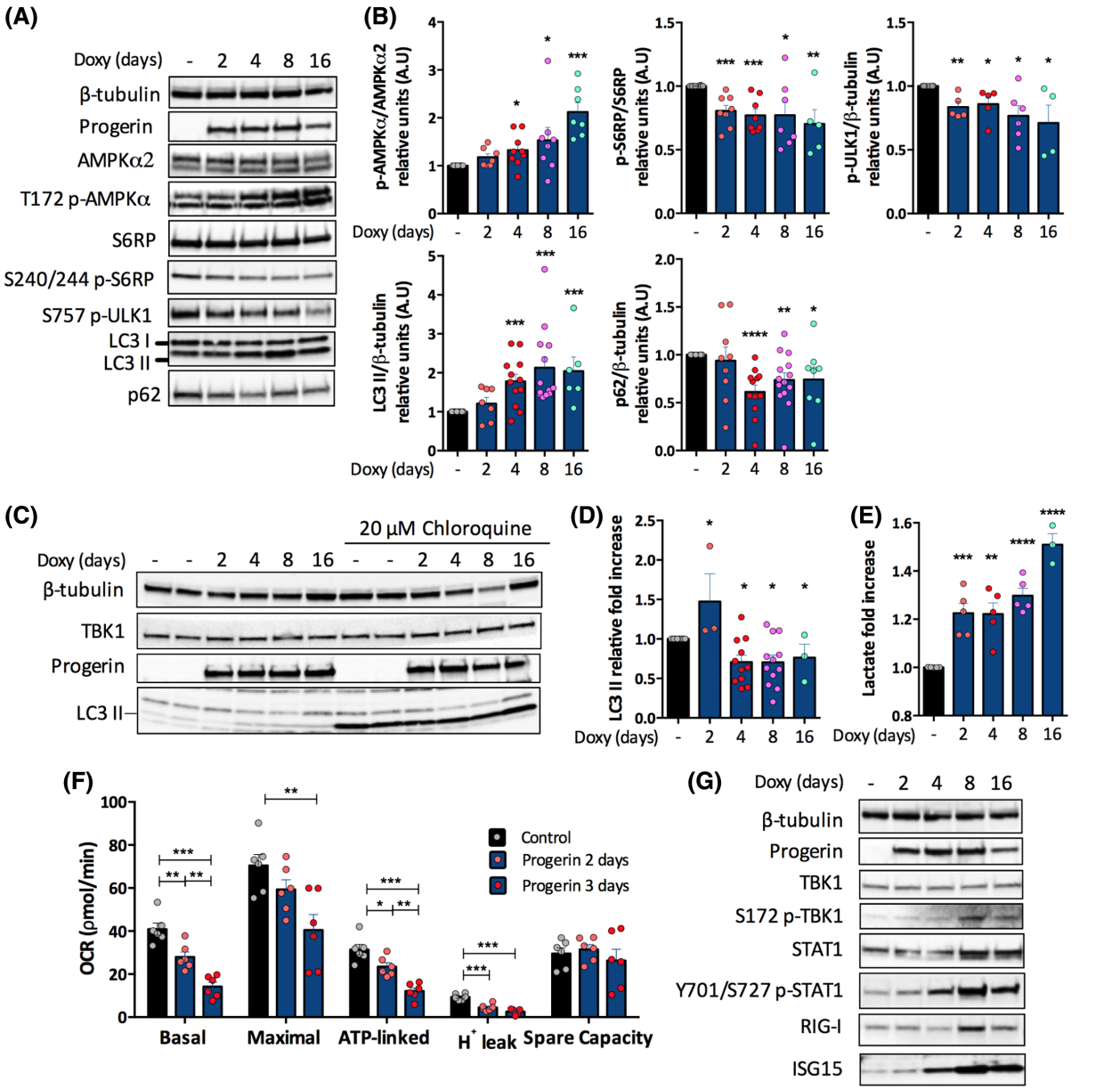

Figure 1. Progerin induces metabolic changes and sterile inflammation in fibroblasts. (A) Immunoblot of doxy-induced GFP-progerin expression in Human Dermal Fibroblasts (HDFs) for 2–16 days detecting GFP-progerin, nutrient sensing proteins (AMPKα and p-AMPKα), mTORC1 target proteins (S6RP, p-S6RP, and p-ULK1), and autophagy markers (LC3-II and p62). β-tubulin was used as loading control (n = 4–10) and DMSO as vehicle treatment in control samples. (B) Densitometry of immunoblots showing average ±SEM from 4 to 12 biological repeats. (C) Immunoblot of doxy-induced GPF-progerin expression in HDFs for 2–16 days and DMSO-treated cells for 2 and 16 days. Cells were treated with 20 μM chloroquine to block autophagy flux and LC3-II was used as an autophagy marker. β-tubulin and TBK1 were used as loading controls (n = 3–12). (D) Densitometry of immunoblots showing LC3-II relative fold increase after chloroquine treatment. (E) Extracellular l-lactate level in culture media of DMSO-treated and doxy-treated HDFs for 2–16 days. (F) Seahorse-measured oxygen consumption rate (OCR) in HDFs treated with doxy for 1 or 2 days and 24 hours of doxy release, resulting in 2 or 3 days of progerin expression, respectively. Respiration parameters were calculated, and three independent experiments were performed with six technical replicates each. One representative experiment (out of three) is shown in the graph. (G) Immunoblot analysis for sterile inflammation markers (TBK1 and p-TBK1, STAT1 and p-STAT1, RIG-I and ISG15) was performed in HDFs expressing GFP-progerin for 2–16 days. Densitometry can be found in **Figure S1C**. The experiments represent 3–15 biological repeats, and β-tubulin was used as loading control. In all experiments and all figures: *p < 0.05, **p < 0.01, ***p < 0.001, ****p < 0.0001.

active form of vitamin D_3. The rationale for this is that we have previously shown that calcitriol rescues or at least ameliorates most phenotypes of progerin-expressing cells, including DNA replication and repair defects, nuclear abnormalities, senescence hallmarks, and most important for this study, sterile inflammation/IFN-like response[29,30,34]. Calcitriol repression of the IFN response in progerin-expressing cells is evidenced by the reduced levels of STAT1 phosphorylation (tyrosine 701 and serine 727) and expression of ISGs such as RIG-I, STAT1, and ISG15 at protein (Fig. 2A and **Fig. S2A**) and transcript (Fig. 2B) levels. Interestingly, calcitriol also reduces TBK1 activation/phosphorylation (serine 172) (Fig. 2A and **Fig. S2A**) and the expression of inflammatory

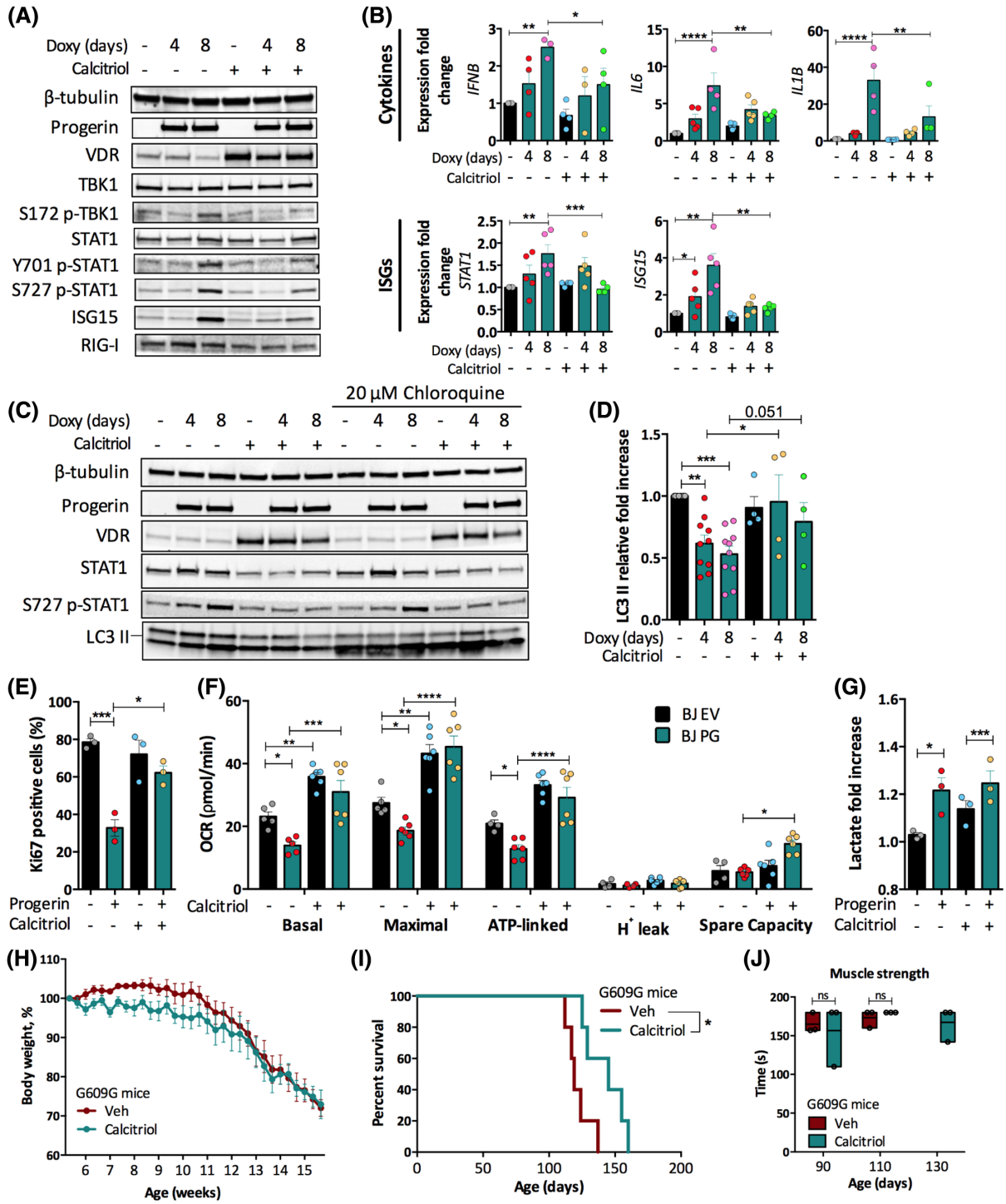

Figure 2. Calcitriol mitigates aging phenotypes in progerin-expressing fibroblasts and extends progeria mice longevity. In panels (A–D), HDFs with doxy-induced GFP-progerin expression for 4 and 8 days treated with calcitriol (active form of vitamin D_3) or vehicle (fetal bovine serum [FBS]). (A) Immunoblot of sterile inflammation markers, such as TBK1/p-TBK1, STAT1/p-STAT1, RIG-I, and ISG15. Densitometry can be found in **Figure S2A**. Vitamin D receptor (VDR) was used to validate calcitriol treatment and β-tubulin as loading control (n = 3–8). (B) Quantitative reverse-transcription real-time PCR (qRT-PCR) of transcripts encoding inflammatory cytokines (*IFNB*, *IL6*, and *IL1B*) and interferon (IFN)-stimulated genes (ISGs) (*STAT1* and *ISG15*) were monitored in three to five independent experiments. (C) Autophagy measurement using immunoblot of LC3-II marker. Cells received 20 μM chloroquine to block autophagy flux. β-tubulin was the loading control (n = 4–9). (D) Immunoblot quantification showing LC3-II relative fold increase after chloroquine treatment. In panels (E–G), BJ fibroblasts expressing progerin (BJ PG) or carrying an empty vector (BJ EV) were treated with calcitriol or vehicle (FBS) for 2 days. (E) Proliferative capacity measurement: immunofluorescence quantification (**Fig. S2B**) of percentage of Ki67 positive cells (n = 3). (F) OCR measurement in cells using Seahorse. Respiration parameters were calculated, and one representative experiment (out of three) is shown in the graph. (G) Extracellular l-lactate level in culture media relative to controls. Graph shows three independent biological repeats. (H) Body weight percentage of female G609G mice receiving calcitriol/cholecalciferol-D_3 treatment or vehicle (Veh) and (I) their Kaplan–Meier survival curves (n = 5). Median survival in calcitriol-treated mice is 145 days and 119 days in vehicle-treated mice, 22% improvement (log-rank test). (J) Graphs showing latency to fall (seconds) of chow-fed G609G mice treated with calcitriol or vehicle at 90, 110, and 130 days of age.

cytokines such as *IFNB*, *IL6*, and *IL1B* (Fig. 2B), which are classical factors of the senescence-associated secretory phenotype[48].

In addition, calcitriol treatment improves autophagy flux (Fig. 2C,D and **Fig. S2B**) and proliferative capacity when compared with vehicle-treated cells (Fig. 2E and **Fig. S2C**). Importantly, BJ fibroblasts (human fibroblast cell line derived from the foreskin of a newborn) expressing progerin constitutively show similar defects in proliferation (Fig. 2E), mitochondrial function (Fig. 2F and **Fig. S2D**), and glycolysis (Fig. 2G) as HDFs with inducible progerin expression. Calcitriol rescues mitochondrial function and ATP-linked respiration in progerin-expressing BJ fibroblasts but does not prevent the increase in lactate production (Fig. 2G) or decreased mTORC1 activity (**Fig. S2E**), suggesting that these latter phenotypes might help maintain cellular homeostasis in the context of progerin expression. In summary, although calcitriol treatment did not alter nutrient sensing, it restored mitochondrial respiration and improved autophagy flux in progerin-expressing fibroblasts.

Next, we determined whether the benefits of calcitriol in cells translate *in vivo*, improving phenotypes of progeria $Lmna^{G609G/G609G}$ (herein G609G) mice. This mouse model phenocopies the main clinical manifestations of human HGPS, such as shortened lifespan, loss of white adipose tissue (WAT), and bone and cardiovascular abnormalities[49,50]. Progeria mice treated with calcitriol injections and cholecalciferol (vitamin D_3)-enriched diet still displayed weight loss over 15 weeks of age (Fig. 2H), but showed significantly prolonged survival, with median survival of 145 days compared to 119 days in vehicle-treated mice, representing a 22% lifespan increase (Fig. 2I). Furthermore, muscle strength was not affected by the treatment when assessed by wire hang method (Fig. 2J). These data demonstrate the beneficial effects of calcitriol *in vitro* and *in vivo* and suggest a new therapeutic strategy for HGPS patients.

JAK-STAT pathway inhibition represses the IFN response and improves cellular and organismal progeria phenotypes

Despite these calcitriol-associated benefits, the improvement in cellular/organismal health may not be only associated with reduced sterile inflammation due to a wide range of calcitriol targets[29,30,34]. To define the specific contribution of the IFN response to metabolic alterations in cells expressing progerin, we treated the cells with an inhibitor of the JAK-STAT pathway, baricitinib. HDFs expressing progerin and treated with baricitinib showed significant inhibition of STAT1 and TBK1 activation (Fig. 3A and **Fig. S3A**) as well as suppression of expression of cytokines and ISGs (Fig. 3B). These data reveal an important role of baricitinib in both inflammation branches in progeria, inflammatory cytokines, and IFN response.

Furthermore, JAK-STAT signaling inhibition in HDFs expressing progerin significantly improved defects in autophagy flux (Fig. 3C,D and **Fig. S3B**) and proliferation (Fig. 3E). In progerin-expressing BJ fibroblasts, baricitinib also improves proliferative capacity (Fig. 3F and **Fig. S3C**), demonstrating the negative effect of the IFN response pathway on progeria cell growth. Interestingly, targeting JAK-STAT signaling with baricitinib provided significant benefits to mitochondrial function. Baricitinib augmented spare respiratory capacity, basal, maximal, and ATP-linked respiration (Fig. 3G and **Fig. S3D**). However, JAK-STAT inhibition did not affect the increase in lactate induced by progerin (Fig. 3H). Considering that neither calcitriol nor baricitinib treatments normalize the levels of glycolysis or mTORC1 activity (**Figs. S2C and S3E**), it is likely that IFN response-independent mechanisms drive these phenotypes in progeria, and that these changes are cellular responses to maintain cellular homeostasis/health. Taken together, these results reveal the contribution of the JAK-STAT pathway to cellular defects in progeria, and support targeting this pathway for HGPS and other sterile inflammation-related aging disorders.

Next, we tested the impact of baricitinib on progeria mice. We previously demonstrated that feeding G609G mice a high-caloric/high-fat diet (HFD) delays aging phenotypes and nearly doubles their lifespan[15]. Here, we determined the therapeutic benefits of baricitinib in mice fed either standard diet or HFD. We find that baricitinib does not increase body weight of male G609G mice fed standard chow (Fig. 4A). By contrast, baricitinib reduced the decline in body weight in HFD-fed G609G mice (Fig. 4B). In addition, baricitinib prolonged survival of treated mice fed either standard chow or HFD (Fig. 4C). Chow-fed G609G mice treated with baricitinib show 13.4% improvement in median survival when compared with vehicle-treated mice, whereas baricitinib administration in HFD-fed G609G mice extended median survival by 18%. The highest extension in longevity was found in mice receiving the combination of HFD and baricitinib, resulting in 47% improvement in lifespan, with respect to untreated chow-fed mice. Overall, our data support baricitinib as a potential treatment for HGPS and demonstrate the synergistic effect when combined with a fat-rich diet.

Targeting Stat1 extends longevity of progeria mice

Based on the crucial function of Stat1 in the IFN response, we tested its potential role in tissue degeneration by determining whether Stat1 depletion provides therapeutic benefits and mediates baricitinib improvements in progeria mice. We generated male and female G609G mice with Stat1 haploinsufficiency. These G609G, $Stat1^{+/-}$ mice were indistinguishable in terms of body weight from G609G, $Stat1^{+/+}$ mice fed either standard chow (Fig. 4D) or HFD (Fig. 4E). However, median survival of G609G, $Stat1^{+/-}$ mice fed chow diet was increased 15.3% relative to G609G, $Stat1^{+/+}$ mice (Fig. 4F), suggesting that ablating one copy of Stat1 gene in chow-fed G609G mice provides similar therapeutic benefits as baricitinib treatment. This effect was observed in male and female mice (**Fig. S4B,D**). In HFD, however, survival of G609G, $Stat1^{+/-}$ mice was not increased with respect to G609G, $Stat1^{+/+}$ mice (Fig. 4F), with the same results for male and female mice (**Fig. S4F,H**). Interestingly, deletion of both copies of *Stat1* was detrimental, leading to decreased body weight and no improvement in survival of either male or female G609G mice fed standard chow (**Fig. S4A,C**). This is consistent with results in progeria cells, where complete depletion of STAT1 by shRNAs hinders cell survival[29]. For HFD-fed mice, females were particularly sensitive to complete loss of Stat1 (G609G, $Stat1^{-/-}$) (**Fig. S4E,F**), compared to males (**Fig. S4G, H**). Overall, these results demonstrate a critical role for Stat1 driving organismal decline in progeria mice. The effects of Stat1 haploinsufficiency mirror the benefits of a HFD, but they are not additive, suggesting that both approaches may target similar mechanisms. Alternatively, other Stat family members might be mediating the benefits of HFD. Considering the ample spectrum of Stat1-target genes and transcriptional programs, and the data presented here linking Stat1 with organismal decline, we predict that maintaining optimal Stat1 function will be required for positive outcomes in HGPS/antiaging therapy.

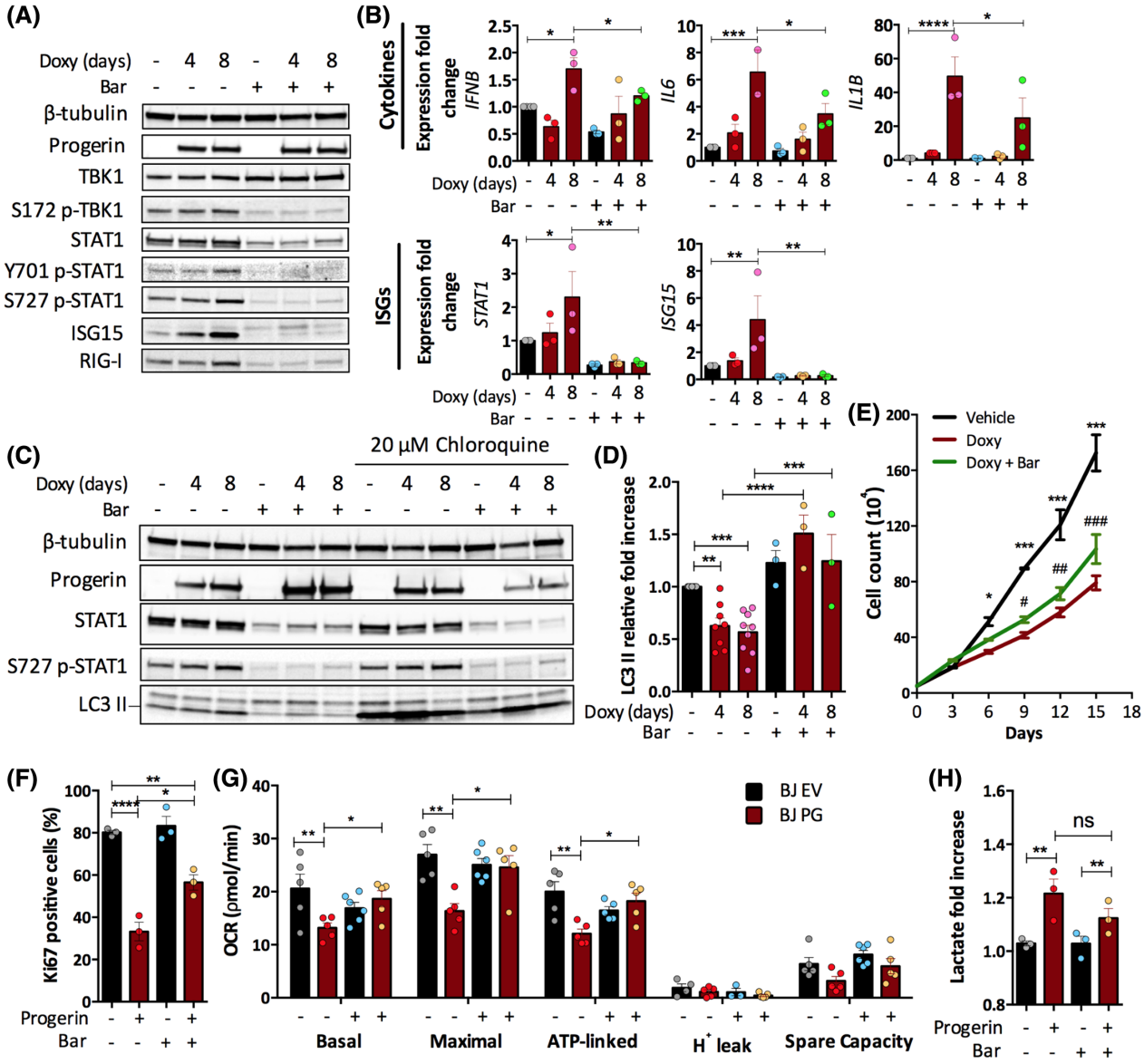

Figure 3. JAK-STAT inhibition using baricitinib improves cellular health of progerin-expressing fibroblasts. In panels (A–D), HDFs with doxy-induced GFP-progerin expression for 4 and 8 days treated with baricitinib (JAK-STAT inhibitor, Bar) or vehicle (DMSO). (A) Immunoblot of sterile inflammation markers, such as TBK1/p-TBK1, STAT1/p-STAT1, RIG-I, and ISG15. β-tubulin was used as loading control, and densitometry can be found in **Figure S3A**. (B) qRT-PCR of transcripts encoding inflammatory cytokines (*IFNB*, *IL6*, and *IL1B*) and ISGs (*STAT1* and *ISG15*) were monitored in three to four biological repeats. (C) Autophagy measurement using immunoblot of LC3-II marker. Cells were treated with 20 μM chloroquine to block autophagy flux and β-tubulin was used as loading control (n = 3–9). (D) Immunoblot quantification showing LC3-II relative fold increase after chloroquine treatment. (E) Cell counting measuring proliferation in high-fat diet (HFD) with doxy-induced GFP-progerin expression treated with vehicle or baricitinib and compared to cells with no doxy addition (n = 3). (*) represents statistical significance between Vehicle and Doxy, and (#) between Doxy and Doxy + Bar groups. In panels (F–H), BJ fibroblasts expressing progerin (BJ PG) or carrying an empty vector (BJ EV) were treated with baricitinib or vehicle (DMSO) for 2 days. (F) Proliferative capacity measurement: immunofluorescence quantification (**Fig. S3B**) of percentage of Ki67 positive cells (n = 3). (G) OCR measurement in cells using Seahorse. Respiration parameters were calculated, and one representative experiment (out of three) is shown in the graph. (H) Extracellular l-lactate level in culture media relative to controls. Graph shows three independent biological repeats.

Targeting Stat1 delays tissue wasting and improves progeria mice health

Progeria mice have characteristics of sarcopenia, such as muscle atrophy and mitochondrial dysfunction, which can lead to weakness[51]. To determine if the Stat1 response contributes to muscle weakness in G609G mice, we monitored muscle strength in mice treated with vehicle or baricitinib and in Stat1 haploinsufficient mice. We did not observe any significant change in muscle strength among groups of mice fed a control chow diet, which die between 90 and 130 days of age (Fig. 4G). However, significantly increased muscle strength in baricitinib-treated and G609G, *Stat1*$^{+/-}$ mice was detectable at later time points due to lifespan extension from HFD-feeding (days 120, 150, and 170; Fig. 4H). These data indicate that the Stat1 pathway contributes to muscle weakness that develops late in G609G mice.

The increase in lifespan of G609G mice fed HFD allows the development of more severe aging phenotypes that better recapitulate human disease, including skin abnormalities, alopecia, and robust VSMC loss in the aorta[14,15]. Interestingly, baricitinib treatment of G609G mice fed HFD delays hair loss, evident at

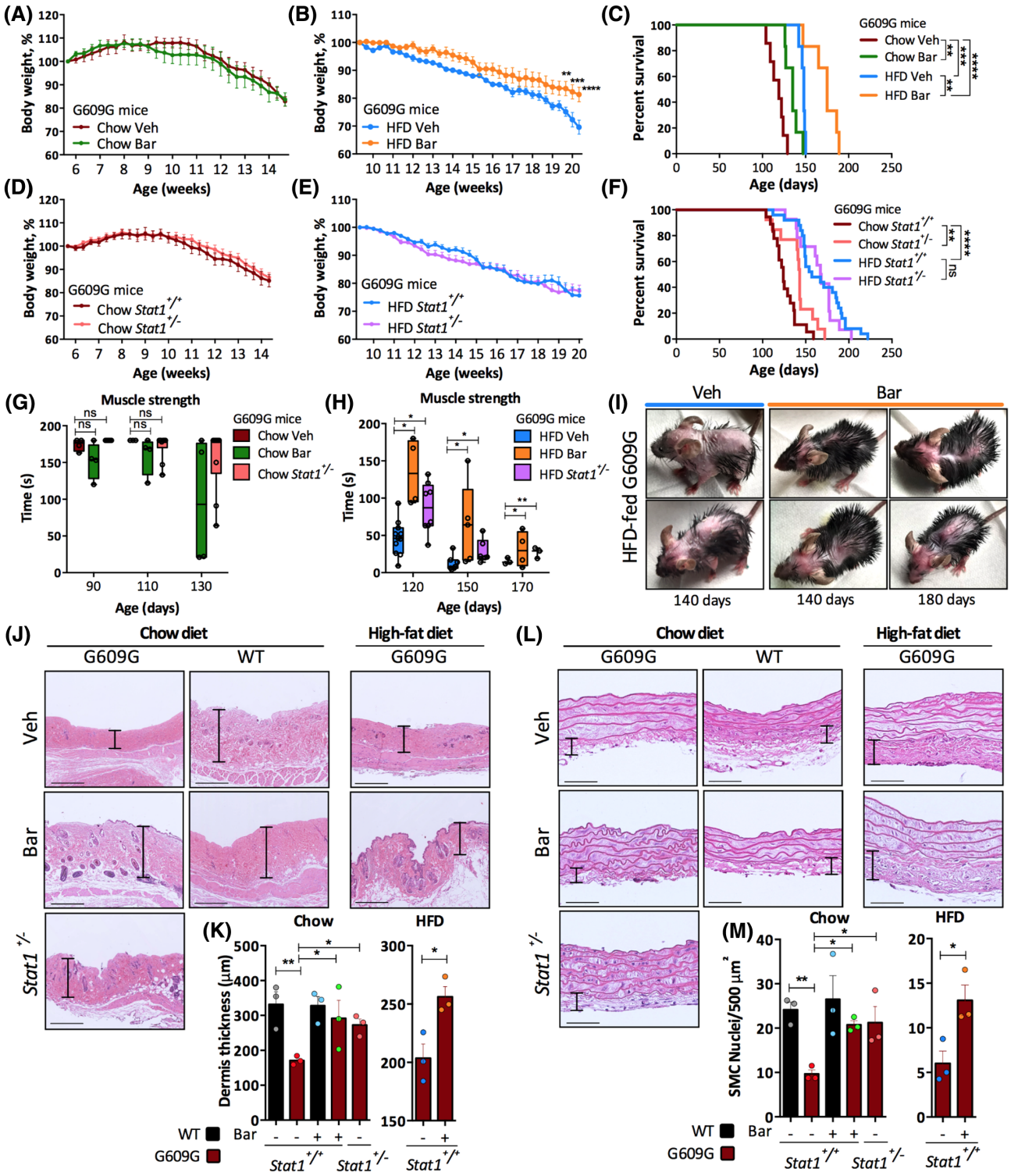

Figure 4. Targeting Stat1 provides significant benefits to progeria mice health and lifespan. (A) Body weight percentage of male G609G mice receiving baricitinib (Bar) treatment or vehicle (Veh), fed a standard chow or (B) high-fat diet (HFD). Mouse body weight was monitored three times a week (n = 6–7 mice/group). (C) Kaplan–Meier survival curves of male G609G mice fed both chow and HFD and treated with vehicle or 30 mg kg^{-1} baricitinib (week dose, n = 6–7 mice/group). Median survival of chow-fed G609G mice is 135 days for baricitinib-treated and 119 days for vehicle-treated mice (13.4% improvement). Median survival in HFD-fed G609G mice treated with baricitinib is 175 days and vehicle 148 days (18% improvement). (D) Body weight percentage of mixed male and female G609G mice homozygous (n = 18) or heterozygous (n = 13) for Stat1 on chow diet or (E) HFD (n = 25 or n = 14, respectively). Mouse body weight was monitored three times a week. (F) Kaplan–Meier survival curves of mixed male and female G609G mice, fed both chow and HFD, and homozygous or heterozygous for *Stat1*. Median survival of chow-fed G609G, $Stat1^{+/-}$ mice (n = 18) is 143 days and 124 days for G609G, $Stat1^{+/+}$ (n = 13, 15% improvement). Median survival of HFD-fed G609G, $Stat1^{+/-}$ mice (n = 25) is 168 days and 157 days for G609G, $Stat1^{+/+}$ (n = 14, no significant improvement). Note that HFD-fed G609G mice injected with vehicle died earlier (~200 days) than the same mice

(legend continued on next page)

not injected, likely due to the three intraperitoneal injections per week. (G) Wire hang, muscle strength test at day 90, 110, and 130 of age in chow-fed male G609G treated with vehicle (n = 4), baricitinib (n = 4), and *Stat1*$^{+/-}$ (n = 4). (H) Wire hang, muscle strength test at day 120, 150, and 170 of age in HFD-fed male G609G treated with vehicle (n = 9), baricitinib (n = 4), and *Stat1*$^{+/-}$ (n = 5). (I) Photographs of male G609G mice fed HFD and treated with vehicle (blue line) or baricitinib (orange line) on day 140 and 180 of age. Hair loss was monitored and compared. (J) Histology of skin with H&E staining of HFD-fed G609G mice treated with vehicle or baricitinib (120 days of age) and chow-fed G609G mice (90 days of age) treated with vehicle, baricitinib or *Stat1*$^{+/-}$. Black bars show the dermis layer of the skin in each picture (500 μm scale). (K) Quantification of dermis thickness in μm (n = 3 mouse skins per group). (L) Histology of aortic arch with H&E staining of HFD-fed G609G mice treated with vehicle or baricitinib (120 days of age) and chow-fed G609G mice (90 days of age) treated with vehicle, baricitinib or *Stat1*$^{+/-}$. Black bars show the adventitia layer of the aorta in each picture (50 μm scale). (M) Quantification of smooth muscle cell (VSMC) nuclei per 500 μm^2 (n = 3 mouse aortas per group).

140 days of age, compared to vehicle-treated mice (Fig. 4I). In fact, long-living mice treated with baricitinib (180 days) still were less alopecic than mice treated with vehicle at 140 days, which suggests a critical role of sterile inflammation in the hair loss. Besides alopecia, JAK-STAT pathway inhibition mitigates skin abnormalities of G609G mice. With aging, there is thinning of the dermis, middle layer of the skin, that is accompanied by decreased vascularity and cellularity[52]. Baricitinib treatment, as well as Stat1 haploinsufficiency, significantly increases the thickness of the dermis of G609G mice fed both diets (Fig. 4J,K).

In addition, we evaluated the effect of Jak-Stat pathway blockage in the aortas of G609G mice, a tissue that shows dramatic degeneration[50,53,54]. Specifically, aortas of G609G mice exhibit almost a complete loss of vascular smooth muscle cells (VSMC) in the medial layer, when compared with aortas of wild-type (WT) mice. G609G mice fed HFD also exhibit a clear thickening of the adventitia layer. Both, baricitinib treatment and Stat1 haploinsufficiency ameliorate the acellularity of aortic tissue in these mice (Fig. 4L,M), with a clear increase in the number of VSMC nuclei. However, we did not observe any difference in adventitia thickness upon baricitinib treatment or Stat1 reduction. These data illustrate the robust effect of baricitinib rescuing specifically the loss of VSMC in the aorta of G609G mice in both diets (Fig. 4M and **Fig. S4I**).

Overall, pharmacological targeting of the STAT1 response improves lifespan and healthspan of progeria mice, even mice fed HFD, which exhibit a more robust phenotype that resembles the severity of human disease. We also demonstrate a specific contribution of Stat1 pathway activation to tissue loss in G609G mice. Altogether, these findings imply that Stat1 is a key driver of aging, tissue degeneration, and organismal decline, and that targeting Stat1 signaling has significant tissue protective effects in progeria.

Stat1 inhibition improves the severe lipodystrophy of progeria mice

White adipose tissue (WAT) undergoes significant loss/degeneration in G609G mice[15,21,37,51,55]. We found that lipoatrophy is significantly delayed by switching mice nutrition to a fat-rich diet[15]. Given the detrimental role of the IFN response in adipogenesis and WAT health[56–58], we investigated whether baricitinib treatment improves WAT homeostasis. Ninety-day-old, chow-fed G609G mice showed pronounced loss of abdominal and subcutaneous fat at necropsy when compared with WT mice (Fig. 5A). By contrast, G609G mice treated with baricitinib displayed a substantial amount of visceral and subcutaneous fat. Similarly, although visceral and subcutaneous WAT is evident in 120-day-old G609G mice fed HFD, baricitinib administration significantly increased fat deposits compared to vehicle-treated G609G mice. Interestingly, Stat1 haploinsufficiency was enough to recapitulate the robust improvement of visceral WAT atrophy in chow-fed G609G mice (Fig. 5A). Moreover, male and female G609G, *Stat1*$^{+/-}$ mice on either diet accumulated more fat content relative to G609G, *Stat1*$^{+/+}$ mice (Fig. 5B).

Concomitant with WAT wasting, we noticed a significantly smaller adipocyte size in the visceral fat from chow-fed G609G mice[15]. Here, we show that baricitinib monotherapy in these mice not only delays epididymal WAT (eWAT) loss but also rescues the normal adipocyte size (Fig. 5C,D). Similarly, the combination of HFD and baricitinib increases adipocyte size in G609G eWAT when compared to vehicle-treated mice. Interestingly, Stat1 depletion in chow-fed G609G mice significantly enlarged the epididymal adipocytes, suggesting that Stat1 is an important mediator of the toxicity of the IFN response to progeria adipocytes.

Histological analysis from eWAT suggests a white-to-brown adipose tissue remodeling (browning) in G609G mice, characteristic of lipodystrophies, as seen by the elevated population of multilocular adipocytes in standard chow- and HFD-fed G609G mice (Fig. 5C,E). Conversely, both chow- and HFD-fed G609G mice treated with baricitinib, as well as ablation of one copy of *Stat1* reduced the percentage of multilocularity in WAT samples, indicating the importance of Stat1 not only in delaying loss of WAT and lipid storage but also in WAT remodeling.

Next, we evaluated mitochondrial function in WAT and skeletal muscle (SKM) of G609G mice fed both diets by high-resolution respirometry. In the soleus of G609G mice, we find a significant reduction of mitochondrial respiration compared to WT mice (**Fig. S5A**), similar to the mitochondrial dysfunction seen in progerin-expressing fibroblasts. Baricitinib treatment or Stat1 haploinsufficiency did not prevent the decrease in mitochondrial respiration. Finally, combined HFD feeding and baricitinib also did not increase SKM respiration in G609G mice (**Fig. S5B**).

Surprisingly, WAT from chow-fed G609G mice displays dramatically enhanced oxygen flux after the addition of substrates that support oxidative phosphorylation and maximal respiration (Fig. 5F). Importantly, this increase in metabolic respiration is driven by the STAT1-mediated IFN-like response because treatment with baricitinib or Stat1 haploinsufficiency normalizes WAT mitochondrial respiration to the levels of WT adipose tissue. Curiously, G609G mice fed HFD do not exhibit this robust increase in mitochondrial respiration (Fig. 5G), suggesting that this phenotype might result from an attempt to compensate for energy/fat deficiency in the WAT. In summary, these results demonstrate deregulation of mitochondrial respiration in G609G mice in a tissue-specific manner, and a critical role for the upregulated Stat1-mediated IFN-like response driving this phenotype, particularly in WAT.

It is important to note the different behavior of WAT mitochondrial respiration in G609G mice fed regular chow or HFD, as feeding the mice HFD was by itself able to prevent this large increase in mitochondrial function/respiration. This agrees with studies showing that HFD decreases mitochondrial function in WAT in other metabolic diseases[59–61]. HFD was not able, however, to normalize adipocyte area or multilocularity, whereas its combination with baricitinib did influence adipocyte size, WAT remodeling, and mitochondrial respiration. These results suggest that HFD provides the energy source necessary to counteract, at least partially and for

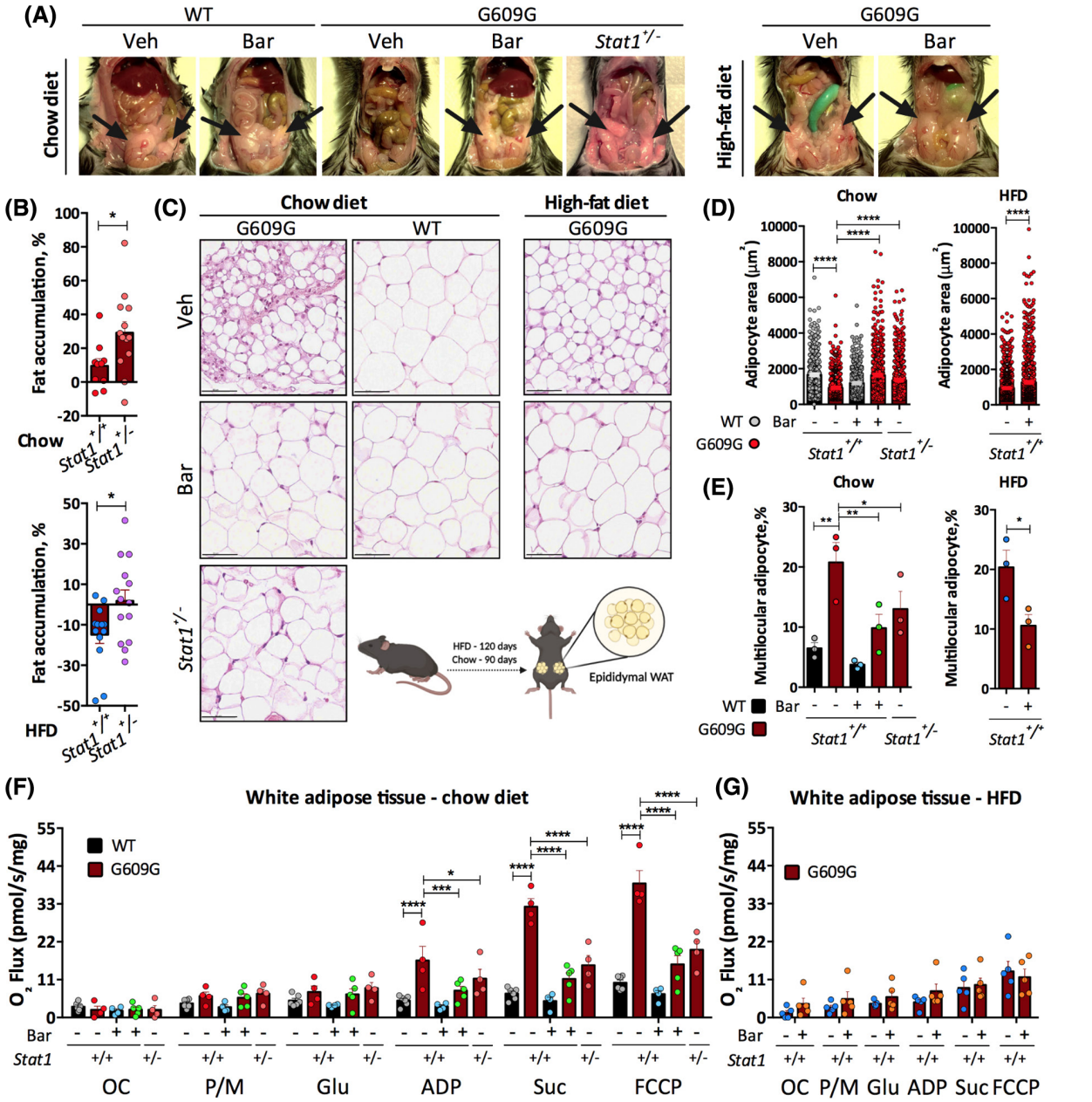

Figure 5. Targeting Stat1 improves adipocyte health and delays lipodystrophy in progeria mice. (A) Pictures show *Lmna*$^{+/+}$ (WT) and G609G mice treated with baricitinib or vehicle and G609G, *Stat1*$^{+/-}$ fed a standard chow (n = 5, 90 days of age), and G609G mice treated with baricitinib or vehicle fed HFD (n = 5, 120 days of age). Gray arrows point to the presence of visceral fat. (B) NMR measurements of percentage of fat accumulation in male and female G609G, *Stat1*$^{+/+}$ and G609G, *Stat1*$^{+/-}$ mice fed standard chow (n = 10–13) or HFD (n = 13–14). Panels (C–G) represent epididymal white adipose tissue (eWAT) analysis of WT and G609G treated with baricitinib or vehicle and G609G, *Stat1*$^{+/-}$ fed a standard chow (90 days of age), and G609G mice treated with baricitinib or vehicle fed HFD (120 days of age). (C) Images from histology of H&E stained eWAT (n = 3 mouse eWAT per group). Bars at the left bottom represent 100 µm scale. (D) Graphs show the quantification of adipocyte size in µm^2 of approximately 400 adipocytes per sample (n = 3). (E) Graphs show the quantification of percentage of multilocular adipocytes in 4–6 random areas per eWAT sample (n = 3). (F) Measurement of mitochondrial respiration using Oroboros instrument of eWAT from mice experimental groups fed a standard chow or (G) HFD. Graphs show average ±SEM of oxygen flux in permeabilized eWAT samples after sequential additions of octanoyl-l-carnitine (OC), pyruvate and malate (P/M), glutamate (G), adenosine diphosphate (ADP), succinate (Suc), and FCCP (n = 4–5).

a period of time, the severe loss of WAT or lipoatrophy in the G609G mice. However, its combination with baricitinib is required for an improvement on adipocyte morphology. Overall, STAT1-mediated IFN response plays a critical role in adipose tissue homeostasis, which might represent an important determinant of healthspan and survival in lipodystrophic diseases.

Discussion

This study defines the toxic relationship between different progeria hallmarks and posits sterile inflammation as one of the pillars of this devastating premature aging disease (Fig. 6). At present, although the only FDA-approved approach for HGPS

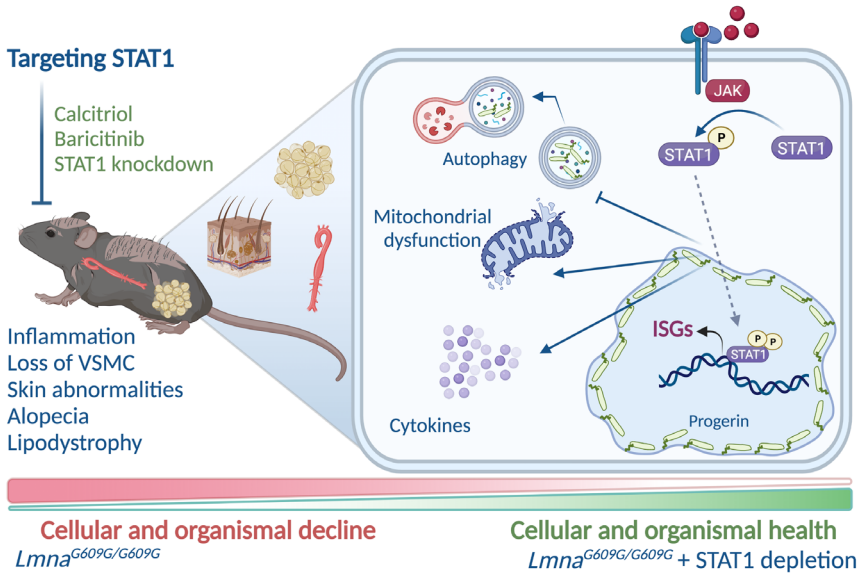

Figure 6. Graphical Abstract. Targeting the STAT1-driven IFN response pharmacologically with calcitriol or baricitinib, or genetically, generating Stat1 haploinsufficiency, improves cellular, tissular, and organismal decline in progeria. At a cellular level, inhibition of STAT1-driven IFN response improves mitochondrial function, ameliorates autophagy flux defects, improves proliferation, and reduces production of pro-inflammatory cytokines. At a tissular level, targeting the pathway improves lipodystrophy, loss of VSMCs in the aorta, and skin aging markers. At an organismal level, increased survival is shown upon targeting the STAT1-driven IFN response.

treatment, a farnesyl transferase inhibitor (Lonafarnib), alleviates some aspects of the disease, it is still not curative. For that reason, our findings on pharmacological and genetic targeting of STAT1 in progeria preclinical models shed light on alternative or combinatorial therapies for HGPS patients.

Over the years, evidence has accumulated indicating that chronic low-level inflammation is a common hallmark of aging and aging-associated disorders, including cardiovascular diseases, atherosclerosis, and lipodystrophy[15,53–55]. Chronic IFN response, for instance, is a harmful mechanism reported in several diseases characterized by increased genomic instability and accelerated aging, such as mitochondrial diseases[3], ataxia telangiectasia[62], and Fanconi anemia[63]. In progeria, studies have shown the contribution of different inflammatory pathways to the disease development and tissue degeneration[35,36,38,64]. We previously showed elevated DNA replication stress eliciting genomic instability, which was accompanied by the upregulation and activation of an IFN-like response[29,30]. Moreover, different compounds reported to improve HGPS phenotypes, including lonafarnib, rapamycin, and calcitriol, rescue replication stress as well as reduce the IFN response, suggesting a detrimental effect of persistent IFN response activation in progeria cells.

Alterations in nuclear architecture, as caused by progerin, induce the loss of vitamin D receptor (VDR) expression, which we find is associated with genomic instability and cellular senescence[34]. Interestingly, VDR knockout mice develop a premature aging phenotype similar to HGPS models, with growth deficiencies and shortened lifespan[65,66]. Calcitriol treatment counteracts VDR loss and mitigates HGPS phenotypes including misshapen cell nuclei, DNA damage, replication stress, cellular senescence, and IFN response[29,30,34]. Here, we find that calcitriol reduces inflammation and ameliorates other aging hallmarks in progerin-expressing cells, including autophagy, mitochondrial function, and cell growth. In addition, our *in vivo* studies reveal that calcitriol administration in G609G mice extends their lifespan by more than 20%, suggesting its potential use in HGPS treatment as a monotherapy or in combination with lonafarnib (Fig. 6).

Comparably to the broad outcomes of calcitriol administration, specific inhibition of the IFN response via JAK-STAT pathway blockage provides advantageous effects to progeria cells. Specifically, pharmacological inhibition of JAK-STAT signaling using baricitinib alleviates inflammation and mitochondrial dysfunction and improves autophagy flux and cell proliferation. Previous studies had shown beneficial effects of baricitinib in HGPS cells and an effect reducing the cellular toxicity associated with lonafarnib[38,39]. Baricitinib is an FDA-approved inhibitor for treating hospitalized COVID-19 patients[67], rheumatoid arthritis[68], and alopecia areata[69]. Our study is the first to demonstrate a robust effect of baricitinib *in vivo*, ameliorating the profound tissue degeneration pathologies associated with HGPS, such as thinning of the skin, alopecia, loss of VSMCs in the aorta, lipodystrophy, muscle weakness, and premature death (Fig. 6). In addition, dual therapy using baricitinib and HFD results in a synergic effect on health and lifespan of G609G mice, extending longevity by about 50% and delaying tissue degeneration. Overall, the results point to STAT proteins as mediators of cellular and organismal aging and posit baricitinib or its combination with HFD as therapeutic alternatives for HGPS patients.

The JAK-STAT pathway serves as a paradigm for cell signaling as well as translational science for common and rare diseases, especially cancer and immune-associated conditions[70]. The ample range of JAK-STAT functions is a result of various stimuli, such as cytokines, IFNs, and growth factors, and different transcriptional programs mediated by seven STAT family members. At present, the JAK inhibitors are categorized based on JAK specificity, which ultimately defines which STAT proteins are efficiently blocked[71]. Therefore, considering simultaneous effects of different STATs in the same disease[72] and the selectivity of JAK-STAT inhibitors[71], molecular characterization of STATs in HGPS

highlights their contribution to the disease development and provides rationale for the application of JAK-STAT blockers as therapies. For instance, studies with STAT1 underscored its importance in mediating Penttinen syndrome[73], Crohn's disease[72], diabetic kidney disease[74], and chronic mucocutaneous candidiasis[75]. Interestingly, here we show that Stat1 reduction in G609G mice mimics baricitinib benefits in mouse health and premature death, unveiling STAT1 as a key mediator of tissue wasting and organismal decline in HGPS.

Taken together, our data demonstrate that STAT1 is a driver of HGPS pathophysiology and sets the path for pharmacological or genetic targeting of STAT1 as alternative treatments for HGPS patients and other diseases driven by an IFN response.

Materials and Methods

Cell culture

HDFs carrying doxycycline-inducible GFP-progerin construct were maintained in Dulbecco's modified Eagle's medium (DMEM) supplemented with 10% fetal bovine serum and 1% antibiotics/antimycotics as described[76] and treated for different time points (2–16 days) with 1 μg mL^{-1} doxycycline or vehicle (DMSO) as control. The cells were treated with either 0.1 μM calcitriol (1α,25-dihydroxyvitamin D3), the hormonally active form of vitamin D, or 1 μM baricitinib 2 days prior the addition of doxycycline. During the treatments, cells were passed when they reached 90% confluence and the culture media supplemented with calcitriol or baricitinib was changed every 2 days. BJ fibroblasts containing constitutive progerin expression vector (pMXIH-G608G) or empty vector (pMXIH-EV) were also treated for 2 days with calcitriol or baricitinib prior the functional experiments, such as mitochondrial function, glycolysis, and cell proliferation.

Mice

The animal studies were conducted in conformity use of laboratory animals and approved by the Institutional Animal Care and Use Committee (IACUC) at Saint Louis University (protocol #2299). The mice used in these studies were housed in a specific pathogen-free facility at a constant temperature of 23 °C with food and water provided *ad libitum* under a 12:12 light–dark cycle. Mice carrying the human HGPS mutation ($Lmna^{G609G/G609G}$) were generated in the laboratory of Carlos Lopez-Otin (C57BL/6 strain). Animals were fed either regular chow or HFD and littermates of the same sex from G609G heterozygous breeders were randomly assigned to experimental groups.

Female $Lmna^{G609G/G609G}$ (G609G) mice were treated with 1 ηg kg^{-1} calcitriol (active form of vitamin D) or vehicle (50% polyethylene glycol 300 in Phosphate-Buffered Saline [PBS]) once a week through intraperitoneal injection, starting at day 40 of age. In addition, on day 80 of age, the regular chow was switched to cholecalciferol-D3 (inactive form of vitamin D, 10,000 IU kg^{-1})-enriched chow. Control mice received vehicle solution and regular chow diet. All experimental groups were monitored for body weight changes and muscle strength, and were euthanized at the humane endpoint.

Baricitinib was administered to G609G mice and $Lmna^{+/+}$ via intraperitoneal injection three times a week, starting at 40 days of age and continued up to the humane endpoint, when the animals were euthanized. Besides monitoring lifespan, chow-fed G609G mice receiving baricitinib or vehicle were sacrificed at day 90 of age and tissues were collected for histological analysis and functional assays. In HFD-fed G609G mice, treatment with baricitinib or vehicle started at day 65 of age and tissue collection was performed at day 120, when the G609G mice start developing a more severe progeroid phenotype. A weekly dosage of 30 mg kg^{-1} of body weight was administered along with vehicle solution (2% DMSO, 30% PEG 300, 5% Tween 80, and ultrapure water). Vehicle solution was injected in parallel to control mice.

For Stat1 depletion studies, Stat1 knockout mice were purchased from the Jackson Laboratory (B6.129S(Cg)-$Stat1^{tm1Dlv}$/J, Strain: #012606). Heterozygous $Lmna^{G609G/+}$ female and male mice carrying one ($Stat1^{+/-}$) or any copy of *Stat1* ($Stat1^{-/-}$) were crossed to obtain G609G, $Stat1^{+/-}$ or G609G, $Stat1^{-/-}$ mice. Body weight was monitored three times a week, and fat composition measured every week by nuclear magnetic resonance (NMR) spectroscopy (the minispec mq 7.5 NMR analyzer-Bruker).

Histology

Mice were euthanized and tissues were collected, washed in PBS, and incubated in 10% formalin. Tissue embedding, sectioning, and staining were performed at HistoWiz. Four-micrometer sections were stained with hematoxylin and eosin (H&E). The aortic arch was excised and cleaned from surrounding fat tissue prior to fixation in 10% formalin. For the analysis of SMC loss, the number of nuclei per 500 μm^2 in the media layer was counted. Histological analysis of WAT was performed in epididymal fat, radial zone. Adipocyte area was measured using ImageJ, and the number of multilocular adipocytes was obtained. Skin was collected from the back of the mice after hair removal using Veer (gel cream hair remover), and the thickness of the dermis was measured using ImageJ.

Wire hang test

In the wire hang testing, mice were placed in a wire mesh, which was slowly inverted 10 inches over a pillow. The latency, or time until the mouse fell off the wire mesh, was recorded.

Immunofluorescence

Cells were grown on coverslips and treated with baricitinib or calcitriol as described. After washing in PBS, cells were fixed with 4% paraformaldehyde for 20 min, permeabilized with 0.1% Triton X-100 in PBS for 10 min, blocked 1 hour at 37°C in 2% Bovine Serum Albumin (BSA)/PBS, stained with primary anti-Ki67 (1:700) overnight and secondary antibody for 2 hours in a humid chamber at 4°C. After washes in PBS, cells were counterstained with 4',6-diamidino-2-phenylindole (DAPI). Microscopy and photo capture were performed on a Leica DM5000B microscope using 63× oil objective lenses with a Leica DFC350FX digital camera and the Leica Application Suite. Ten to fifteen images per sample were acquired and at least 100 cells per genotype were used to obtain statistical significance of Ki67 positivity.

Quantitative reverse-transcription PCR (qRT-PCR)

Total cellular RNA was purified from the cells using Zymo kit according to manufacturer instructions. Total cDNA was obtained by reverse transcription of 0.5 μg total purified RNA using SuperScript VILO cDNA Synthesis kit. Quantitative PCR was performed using the 7500HT Fast Real-Time PCR system with Power SYBR Green PCR Master Mix. Reactions were performed in triplicate, and GAPDH was amplified in the same plate as an internal control. Relative quantitative measurements of target genes were determined by comparing cycle thresholds. List of target genes and sequences is available in Supplemental Materials.

Immunoblotting

Cells were lysed with UREA buffer (8 M Urea, 40 mM Tris pH 7.5, 1% NP40) for 6 hours in ice. The lysates were centrifuged at 14,000 g for 15 min at 4 °C. The supernatants were collected, and 50 μg of total protein was mixed with Laemmli loading buffer. Equal protein amounts were separated by SDS-PAGE on a 4%–15% Criterion TGX Gel (Bio-Rad) and transferred to a nitrocellulose membrane using the Trans-Blot Turbo system (Bio-Rad). Membranes were blocked using 5% BSA in Tris-Buffered Saline (TBS) for 1 hour at room temperature, then incubated overnight at 4 °C with primary antibody diluted in blocking solution. Membranes were washed 3× using TBS+0.1% Tween-20 after both primary and secondary antibody incubations. Membranes were developed using Immobilon Western Chemiluminescent HRP Substrate (Merck Millipore). Densitometric values were determined and quantified on immunoblots at non-saturating exposures using the ImageJ and normalized by one of the housekeeping loading controls.

Autophagy

Autophagic flux was monitored by LC3 turnover using immunoblot, which is based on the observation that LC3-II is degraded in autolysosomes. For autophagy flux inhibition, cells were treated with 20 μM chloroquine for 16 hours or 10 nM bafilomycin A1 for 24 hours prior cell collection. Immunoblot images were taken using a SYNGENE PXi, and the intensity of the protein bands were quantified using ImageJ. Relative fold change of LC3-II is defined as the ratio of LC3-II band intensity, normalized to the housekeeping, in cellular extracts from chloroquine-treated versus non-treated cells.

Cell proliferation

Cells were plated in triplicate in six-well plates at 100,000 cells per well and counted when confluency was near 90% utilizing Trypan Blue Viability Assay on the Nexcelom Cellometer Vision CBL. To extrapolate proliferation to the respective time periods (3, 6, 9, 12, and 15 days), we used the $N_f = N_0 e^{kt}$ equation[34].

L-lactate concentration measurement

Lactate production in HDFs and BJs was measured using an l-lactate assay kit. Prior to the lactate production measurement, cultured cells were incubated for 16 hours with fresh media containing indicated treatments. All measurements were performed three times in triplicate in three independent experiments.

Seahorse assay

A Seahorse XFe96 Bioanalyzer (Agilent) was used to measure mitochondrial respiration. HDFs were treated with DMSO for 24 or 48 hours followed by 24 hours doxycycline/vehicle release, and BJ fibroblasts were treated with either calcitriol or baricitinib 48 hours prior the assay. Briefly, cells were plated at a density of 1×10^4 cells per well in 200 μl of DMEM culture media in Agilent Seahorse XF96 Cell Culture Microplate. Following a 16-hour incubation at 37°C, cells were washed and replaced with prewarmed XF Base Assay media supplemented with 1 mM pyruvate, 2 mM glutamine, and 10 mM glucose (pH 7.4), and incubated at 37°C in a humidified atmosphere without CO_2 for 1 hour. OCR was measured after sequential addition of 1.5 μM oligomycin, 0.5 μM FCCP, 0.5 μM antimycin A + rotenone from the Mitochondrial Stress Test Kit (Agilent). OCR measurements of each well were exported and basal, maximal, ATP-linked, spare, H^+ leak, and non-mitochondrial respiration calculated.

High-resolution respirometry

Mitochondrial respiration in the rostral zone of eWAT was measured using an Oroboros Oxygraph O2k FluoRespirometer (Oroboros Instruments). After excision, adipose samples were immersed in ice-cold BIOPS buffer (50 mM MES, 10 mM EGTA, 6.56 mM $MgCl_2$, 0.5 mM DTT, 20 mM imidazole, 5.77 mM ATP, and 15 mM phosphocreatine, pH 7.1). WAT was then blotted dry, weighed, and minced into approximately 1 mg pieces, which was placed in prewarmed Oroboros chambers with mitochondrial respiration solution MiR05 (3 mM $MgCl_2$, 0.5 mM EGTA, 20 mM taurine, 60 mM k-lactobionate, 10 mM KH_2PO_4, 110 mM sucrose, 20 mM HEPES, and 1 g L^{-1} BSA, pH 7.1). For sample permeabilization, 2 μM digitonin was added to each chamber, and oxygen was provided to ensure O_2 availability within the tissue pieces. In order to measure O_2 flux, different substrates were sequentially added: 1.5 mM octanoyl carnitine, 5 mM pyruvate, 10 mM glutamate, and 2 mM malate, 20 mM ADP, and 20 mM succinate, followed by three pulses of 0.5 μM FCCP. O_2 flux per mass was recorded using DatLab 7.4 software.

For mitochondrial respiration analyses in muscles, soleus was excised from the mice and immersed in an ice-cold solubilization solution containing 5 mg mL^{-1} saponin in BIOPS buffer for 30 min at 4 °C. Samples were then placed in MiRO5 buffer for additional 30 min prior preparation. Solubilized soleus was minced into 1-mg pieces and placed into the Oroboros chambers filled with MiRO5 buffer, 3 mg mL^{-1} creatine, and 2 uM blebbistatin. Chambers were hyperoxygenized to prevent O_2 concentrations from limiting O_2 flux measurements. O_2 flux measurements were then performed with substrate additions as previously described for WAT.

RNA sequencing

Detailed RNA sequencing procedure is described previously[29]. In this study, the levels of transcripts encoding glycolytic enzymes between five lines of normal fibroblasts (from the parents of patients with HGPS) and three different lines of HGPS were compared.

Statistical analysis

One-way or two-way analysis of variance (ANOVA) was used for the experiments in which more than two comparisons were performed; if $p < 0.05$, significance between groups was determined using post hoc analysis. For comparisons between groups, Student's t test was used with Bonferroni correction. Error bars displayed throughout this article represent standard error of the mean (SEM) and were obtained from replicates of each biological sample unless otherwise indicated. Survival curves were generated using the Kaplan–Meier method and log-rank test to determine statistical significance between survival differences. GraphPad Prism 8.02 was used for the calculations. In all cases, differences were considered statistically significant, when $p < 0.05$ (*$p < 0.05$, **$p < 0.01$, ***$p < 0.001$, ****$p < 0.0001$).

Acknowledgments

Funding: National Institutes of Health grant R01AG058714 (S.G.). **Author contributions:** Conceptualization by R.C.F., E.V.S., A.B., K.S.M., C.F., and S.G. Methodology by R.C.F., E.V.S., K.S.M., and C.F. Investigation by R.C.F. and E.V.S. Visualization

by R.C.F. and E.V.S. Supervision by S.G. Writing—original draft by R.C.F. Writing—review and editing by R.C.F., E.V.S., and S.G.

Declaration of Interests

All authors declare that they have no competing interests.

Data Availability Statement

All data are available in the main text or the supplementary materials.

Supplemental Information

Further details, antibody dilutions, primers, and an outline of resources used in this work can be found in the supplemental information, which can be found at https://doi.org/10.59368/agingbio.20230009.

Accepted May 7, 2023
Published June 28, 2023

References

1. López-Otín C., Blasco M.A., Partridge L., Serrano M., & Kroemer G. (2013). The hallmarks of aging. *Cell* **153**(6), 1194–1217. PMID: 23746838; doi: 10.1016/j.cell.2013.05.039.
2. Dou Z., Ghosh K., Vizioli M.G., … Adams P.D., & Berger S.L. (2017). Cytoplasmic chromatin triggers inflammation in senescence and cancer. *Nature* **550**, 402–406. PMID: 28976970; doi: 10.1038/nature24050.
3. Lei Y., Guerra Martinez C., Torres-Odio S., … West L.C., & West A.P. (2021). Elevated type I interferon responses potentiate metabolic dysfunction, inflammation, and accelerated aging in mtDNA mutator mice. *Sci. Adv.* **7**, eabe7548. PMID: 34039599; doi: 10.1126/sciadv.abe7548.
4. Yu C.-H., Davidson S., Harapas C.R., … Crouch P.J., & Masters S.L. (2020). TDP-43 Triggers Mitochondrial DNA Release via mPTP to Activate cGAS/STING in ALS. *Cell* **183**, 636–649.e18.
5. Zheng Y., Gardner S.E., & Clarke M.C.H (2011). Cell death, damage-associated molecular patterns, and sterile inflammation in cardiovascular disease. *Arterioscler. Thromb. Vasc. Biol.* **31**(12), 2781–2786. PMID: 22096097; doi: 10.1161/ATVBAHA.111.224907.
6. Roy E.R., Wang B., Wan Y., … Zheng H., & Cao W. (2020). Type I interferon response drives neuroinflammation and synapse loss in Alzheimer disease. *J. Clin. Investig.* **130**, 1912–1930. PMID: 31917687; doi: 10.1172/JCI133737.
7. Pham P.T., Fukuda D., Nishimoto S., … Barber G.N. & Sata M. (2021). STING, a cytosolic DNA sensor, plays a critical role in atherogenesis: A link between innate immunity and chronic inflammation caused by lifestyle-related diseases. *Eur. Heart J.* **42**(42), 4336–4348. PMID: 34226923; doi: 10.1093/eurheartj/ehab249.
8. Karakasilioti I., Kamileri I., Chatzinikolaou G., … Niedernhofer L.J. & Garinis G.A. (2013). DNA damage triggers a chronic autoinflammatory response, leading to fat depletion in NER progeria. *Cell Metab.* **18**(3), 403–415. PMID: 24011075; doi: 10.1016/j.cmet.2013.08.011.
9. Bai J., Cervantes C., Liu J., … Dong L.Q., & Liu F. (2017). DsbA-L prevents obesity-induced inflammation and insulin resistance by suppressing the mtDNA release-activated cGAS-cGAMP-STING pathway. *Proc. Natl. Acad. Sci. U.S.A.* **114**, 12196–12201. PMID: 29087318; doi: 10.1073/pnas.1708744114.
10. Picca A., Lezza A.M.S., Leeuwenburgh C., … Bernabei R., & Marzetti E. (2018). Circulating mitochondrial DNA at the crossroads of mitochondrial dysfunction and inflammation during aging and muscle wasting disorders. *Rejuvenation Res.* **21**(4), 350–359. PMID: 29125070; doi: 10.1089/rej.2017.1989.
11. McBride M.J., Foley K P., D'Souza D.M., … Hawke T.J., & Schertzer J.D. (2017). The NLRP3 inflammasome contributes to sarcopenia and lower muscle glycolytic potential in old mice. *Am. J. Physiol.-Endocrinol. Metab.* **313**(2), E222–E232. PMID: 28536183; doi: 10.1152/ajpendo.00060.2017.
12. Gordon L.B., Rothman F.G., López-Otín C., & Misteli T. (2014). Progeria: A paradigm for translational medicine. *Cell* **156**(3), 400–407. PMID: 24485450; doi: 10.1016/j.cell.2013.12.028.
13. McClintock D., Ratner D., Lokuge M., … Collins F.S., & Djabali K. (2007). The mutant form of lamin A that causes Hutchinson-Gilford progeria is a biomarker of cellular aging in human skin. *PLoS One* **2**(12), e1269. PMID: 18060063; doi: 10.1371/journal.pone.0001269.
14. Kreienkamp R., & Gonzalo S. (2020). Metabolic dysfunction in Hutchinson–Gilford progeria syndrome. *Cells* **9**(2), 395. PMID: 32046343; doi: 10.3390/cells9020395.
15. Kreienkamp R., Billon C., Bedia-Diaz G., … Burris T.P., & Gonzalo S. (2019). Doubled lifespan and patient-like pathologies in progeria mice fed high-fat diet. *Aging Cell* **18**, e12852. PMID: 30548460; doi: 10.1111/acel.12852.
16. Collins F.S. (2016). Seeking a cure for one of the rarest diseases: Progeria. *Circulation* **134**(2), 126–129. PMID: 27400897; doi: 10.1161/CIRCULATIONAHA.116.022965.
17. Gonzalo S., Kreienkamp R., & Askjaer P. (2017). Hutchinson-Gilford progeria syndrome: A premature aging disease caused by LMNA gene mutations. *Ageing Res. Rev.* **33**, 18–29. PMID: 27374873; doi: 10.1016/j.arr.2016.06.007.
18. Kubben N., & Misteli T. (2017). Shared molecular and cellular mechanisms of premature ageing and ageing-associated diseases. *Nat. Rev. Mol. Cell Biol.* **18**(10), 595–609. PMID: 28792007; doi: 10.1038/nrm.2017.68.
19. Wiley C.D. & Campisi J. (2021). The metabolic roots of senescence: Mechanisms and opportunities for intervention. *Nat. Metab.* **3**(10), 1290–1301. PMID: 34663974; doi: 10.1038/s42255-021-00483-8.
20. Rivera-Torres J., Acín-Perez R., Cabezas-Sánchez P., … Luque-García J.L., & Andrés V. (2013). Identification of mitochondrial dysfunction in Hutchinson-Gilford progeria syndrome through use of stable isotope labeling with amino acids in cell culture. *J. Proteomics* **91**, 466–477. PMID: 23969228; doi: 10.1016/j.jprot.2013.08.008.
21. Lopez-Mejia I.C., de Toledo M., … Casas F., & Tazi J. (2014). Antagonistic functions of LMNA isoforms in energy expenditure and lifespan. *EMBO Rep.* **15**, 529–539. PMID: 24639560; doi: 10.1002/embr.201338126.
22. Maynard S., Hall A., Galanos P., … Maya-Mendoza A., & Bartek J. (2022). Lamin A/C impairments cause mitochondrial dysfunction by attenuating PGC1α and the NAMPT-NAD+ pathway. *Nucleic Acids Res.* **50**(17), 9948–9965. PMID: 36099415; doi: 10.1093/nar/gkac741.
23. Gabriel D., Roedl D., Gordon L.B., & Djabali K. (2015). Sulforaphane enhances progerin clearance in Hutchinson-Gilford progeria fibroblasts. *Aging Cell* **14**(1), 78–91. PMID: 25510262; doi: 10.1111/acel.12300.
24. Evangelisti C., Cenni V., & Lattanzi G. (2016). Potential therapeutic effects of the MTOR inhibitors for preventing ageing and progeria-related disorders. *Br. J. Clin. Pharmacol.* **82**(5), 1229–1244. PMID: 26952863; doi: 10.1111/bcp.12928.
25. Cabral W.A., Tavarez U.L., Beeram I., … Erdos M.R., & Collins F.S. (2021). Genetic reduction of mTOR extends lifespan in a mouse model of Hutchinson-Gilford progeria syndrome. *Aging Cell* **20**, PMID: 34453483; doi: 10.1111/acel.13457.
26. Kychygina A., Dall'Osto M., Allen J.A.M., … Pickett H.A., & Crabbe L. (2021). Progerin impairs 3D genome organization and induces fragile telomeres by limiting the dNTP pools. *Sci. Rep.* **11**(1), 13195. PMID: 34162976; doi: 10.1038/s41598-021-92631-z.
27. Li Y., Zhou G., Bruno I.G., … Cooke J.P., & Shay J.W. (2019). Transient introduction of human telomerase mRNA improves hallmarks of progeria cells. *Aging Cell* **18**, PMID: 31152494; doi: 10.1111/acel.12979.

28. Aguado J., Sola-Carvajal A., Cancila V., … Eriksson M., & d'Adda di Fagagna F. (2019). Inhibition of DNA damage response at telomeres improves the detrimental phenotypes of Hutchinson–Gilford progeria syndrome. *Nat. Commun.* **10**(1), 4990. PMID: 31740672; doi: 10.1038/s41467-019-13018-3.

29. Kreienkamp R., Graziano S., Coll-Bonfill N., … Batista L.F.Z., & Gonzalo S. (2018). A Cell-intrinsic interferon-like response links replication stress to cellular aging caused by progerin. *Cell Rep.* **22**, 2006–2015. PMID: 29466729; doi: 10.1016/j.celrep.2018.01.090.

30. Coll-Bonfill N., Cancado de Faria R., Bhoopatiraju S., & Gonzalo S. (2020). Calcitriol prevents RAD51 loss and cGAS-STING-IFN response triggered by progerin. *Proteomics* **20**(5-6), 1800406. PMID: 31834988; doi: 10.1002/pmic.201800406.

31. Gonzalo S., & Coll-Bonfill N. (2019). Genomic instability and innate immune responses to self-DNA in progeria. *Geroscience* **41**(3), 255–266. PMID: 31280482; doi: 10.1007/s11357-019-00082-2.

32. Zhao Y., Simon M., Seluanov A., & Gorbunova V. (2022). DNA damage and repair in age-related inflammation. *Nat. Rev. Immunol.* **23**(2), 75–89. PMID: 35831609; doi: 10.1038/s41577-022-00751-y.

33. Crow Y.J., & Stetson D.B. (2022). The type I interferonopathies: 10 years on. *Nat. Rev. Immunol.* **22**(8), 471–483. PMID: 34671122; doi: 10.1038/s41577-021-00633-9.

34. Kreienkamp R., Croke M., Neumann M.A., … Carlberg C., & Gonzalo S. (2016). Vitamin D receptor signaling improves Hutchinson-Gilford progeria syndrome cellular phenotypes. *Oncotarget* **7**(21), 30018–30031. PMID: 27145372; doi: 10.18632/oncotarget.9065.

35. Griveau A., Wiel C., Ziegler D.v., Bergo M.O., & Bernard D. (2020). The JAK1/2 inhibitor ruxolitinib delays premature aging phenotypes. *Aging Cell* **19**, e13122. PMID: 32196928; doi: 10.1111/acel.13122.

36. González-Dominguez A., Montañez R., Castejón-Vega B, … Alcocer-Gómez E., & Cordero M.D. (2021). Inhibition of the NLRP3 inflammasome improves lifespan in animal murine model of Hutchinson–Gilford progeria. *EMBO Mol. Med.* **13**, e14012. PMID: 34448355; doi: 10.15252/emmm.202114012.

37. Squarzoni S., Schena E., Sabatelli P., … Zaghini A., & Lattanzi G. (2021). Interleukin-6 neutralization ameliorates symptoms in prematurely aged mice. *Aging Cell* **20**, e13285. PMID: 33393189; doi: 10.1111/acel.13285.

38. Arnold R., Vehns E., Randl H., & Djabali K. (2021). Baricitinib, a JAK-STAT inhibitor, reduces the cellular toxicity of the farnesyltransferase inhibitor Lonafarnib in progeria cells. *Int. J. Mol. Sci.* **22**(14), 7474. PMID: 34299092; doi: 10.3390/ijms22147474.

39. Liu A., & Djabali H. (2019). Inhibition of JAK-STAT signaling with Baricitinib reduces inflammation and improves cellular homeostasis in progeria cells. *Cells* **8**(10), 1276. PMID: 31635416; doi: 10.3390/cells8101276.

40. Kawakami Y., Hambright W.S., Takayama K., … Niedernhofer L.J., & Huard J. (2019). Rapamycin rescues age-related changes in muscle-derived stem/progenitor cells from progeroid mice. *Mol. Ther. Methods Clin. Dev.* **14**, 64–76. PMID: 31312666; doi: 10.1016/j.omtm.2019.05.011.

41. Lee Y.H., Park J.Y., Lee H., … Park J.T., & Park S.C. (2021). Targeting mitochondrial metabolism as a strategy to treat senescence. *Cells* **10**(11), 3003. PMID: 34831224; doi: 10.3390/cells10113003.

42. Abe T., & Barber G.N. (2014). Cytosolic-DNA-mediated, STING-dependent proinflammatory gene induction necessitates canonical NF-κB activation through TBK1. *J. Virol.* **88**(10), 5328–5341. PMID: 24600004; doi: 10.1128/JVI.00037-14.

43. Yan S., Kumari M., Xiao H, … Ahmad R., & Rosen E.D. (2021). IRF3 reduces adipose thermogenesis via ISG15-mediated reprogramming of glycolysis. *J. Clin. Investig.* **131**, e144888. PMID: 33571167; doi: 10.1172/JCI144888.

44. Huffaker T.B., Ekiz H.A., Barba C.1074208, …Voth W.P., & O'Connell R.M. (2021). A Stat1 bound enhancer promotes Nampt expression and function within tumor associated macrophages. *Nat. Commun.* **12**(1), 2620. PMID: 33976173; doi: 10.1038/s41467-021-22923-5.

45. Hasan M., Gonugunta V.K., Dobbs N., … DeBerardinis R.J., & Yan N. (2017). Chronic innate immune activation of TBK1 suppresses mTORC1 activity and dysregulates cellular metabolism. *Proc. Natl. Acad. Sci. U.S.A.*. **114**, 746–751. PMID: 28069950; doi: 10.1073/pnas.1611113114.

46. Alcalá S., Sancho P., Martinelli P., … Hermann P.C., & Sainz B. (2020). ISG15 and ISGylation is required for pancreatic cancer stem cell mitophagy and metabolic plasticity. *Nat. Commun.* **11**(1), 2682. PMID: 32472071; doi: 10.1038/s41467-020-16395-2.

47. Zhao P., In Wong K., Sun X., … Skorobogatko Y., & Saltiel A.R. (2018). TBK1 at the crossroads of inflammation and energy homeostasis in adipose tissue. *Cell* **172**, 731–743.e12. PMID: 29425491; doi: 10.1016/j.cell.2018.01.007.

48. Kumari R., & Jat P. (2021). Mechanisms of cellular senescence: Cell cycle arrest and senescence associated secretory phenotype. *Front. Cell Dev. Biol.* **9**, 645593. PMID: 33855023; doi: 10.3389/fcell.2021.645593.

49. Hamczyk M.R., del Campo L., & Andrés V. (2018). Aging in the cardiovascular system: Lessons from Hutchinson-Gilford progeria syndrome. *Annu. Rev. Physiol.* **80**(1), 27–48. PMID: 28934587; doi: 10.1146/annurev-physiol-021317-121454.

50. Osorio F.G., Navarro C.L., Cadiñanos J., … Lévy N., & López-Otín C. (2011). Splicing-directed therapy in a new mouse model of human accelerated aging. *Sci. Transl. Med.* **3**, PMID: 22030750; doi: 10.1126/scitranslmed.3002847.

51. Zaghini A., Sarli G., Barboni C. … Lattanzi G., & Squarzoni S. (2020). Long term breeding of the Lmna G609G progeric mouse: Characterization of homozygous and heterozygous models. *Exp. Gerontol.* **130**, 110784. PMID: 31794853; doi: 10.1016/j.exger.2019.110784.

52. Quan T., & Fisher G.J. (2015). Role of age-associated alterations of the dermal extracellular matrix microenvironment in human skin aging: A mini-review. *Gerontology* **61**(5), 427–434. PMID: 25660807; doi: 10.1159/000371708.

53. Hamczyk M.R., Villa-Bellosta R., Quesada V., … López-Otín C., Andrés V. (2019). Progerin accelerates atherosclerosis by inducing endoplasmic reticulum stress in vascular smooth muscle cells. *EMBO Mol. Med.* **11**, e9736. PMID: 30862662; doi: 10.15252/emmm.201809736.

54. Sánchez-López A., Espinós-Estévez C., González-Gómez C., … Benedicto I., & Andrés V. (2021). Cardiovascular progerin suppression and lamin A restoration rescue Hutchinson-Gilford progeria syndrome. *Circulation* **144**(22), 1777–1794. PMID: 34694158; doi: 10.1161/CIRCULATIONAHA.121.055313.

55. Revêchon G., Viceconte N., McKenna T., … Franco I., & Eriksson M. (2017). Rare progerin-expressing preadipocytes and adipocytes contribute to tissue depletion over time. *Sci. Rep.* **7**, 1–12. PMID: 28667315; doi: 10.1038/s41598-017-04492-0.

56. Lee K., Um S.H., Rhee D.K., & Pyo S. (2016). Interferon-alpha inhibits adipogenesis via regulation of JAK/STAT1 signaling. *Biochim. Biophys. Acta Gen. Subj.* **1860**(11), 2416–2427. PMID: 27424923; doi: 10.1016/j.bbagen.2016.07.009.

57. Cox A.R., Chernis N., Bader D.A., … Putluri N., & Hartig S.M. (2020). STAT1 dissociates adipose tissue inflammation from insulin sensitivity in obesity. *Diabetes* **69**(12), 2630–2641. PMID: 32994273; doi: 10.2337/db20-0384.

58. Richard A.J., & Stephens J.M. (2011). Emerging roles of JAK–STAT signaling pathways in adipocytes. *Trends Endocrinol. Metab.* **22**(8), 325–332. PMID: 21561789; doi: 10.1016/j.tem.2011.03.007.

59. Rong J.X., Qiu Y., Hansen M.K., Zhu L., … Strum J.C., & Ryan T.E. (2007). Adipose mitochondrial biogenesis is suppressed in db/db and high-fat diet–fed mice and improved by rosiglitazone. *Diabetes* **56**(7), 1751–1760. PMID: 17456854; doi: 10.2337/db06-1135.

60. Choi M.-S., Kim Y.-J., Kwon E.-Y., Ryoo J.Y., Kim S.R., & Jung U.J. (2015). High-fat diet decreases energy expenditure and expression of genes controlling lipid metabolism, mitochondrial function and skeletal system development in the adipose tissue, along with increased expression of extracellular matrix remodelling- and inflammation-related genes. *Br. J. Nutr.* **113**(6), 867–877. PMID: 25744306; doi: 10.1017/S0007114515000100.

61. Schöttl T., Kappler L., Fromme T., & Klingenspor M. (2015). Limited OXPHOS capacity in white adipocytes is a hallmark of obesity in

laboratory mice irrespective of the glucose tolerance status. *Mol Metab*. **4** (9), 631–642. PMID: 26413469; doi: 10.1016/j.molmet.2015.07.001.

62. Härtlova A., Erttmann S.F., Am Raffi F., … Weiss S., & Gekara N.O. (2015). DNA damage primes the type I interferon system via the cytosolic DNA sensor STING to promote anti-microbial innate immunity. *Immunity* **42**(2), 332–343. PMID: 25692705; doi: 10.1016/j.immuni.2015.01.012.
63. Brégnard C., Guerra J., Déjardin S., Passalacqua F., Benkirane M., & Laguette N. (2016). Upregulated LINE-1 activity in the Fanconi anemia cancer susceptibility syndrome leads to spontaneous pro-inflammatory cytokine production. *EBioMedicine* **8**, 184–194. PMID: 27428429; doi: 10.1016/j.ebiom.2016.05.005.
64. Osorio F.G., Bárcena C., Soria-Valles C., … Freije J.M.P., & López-Otín C. (2012). Nuclear lamina defects cause ATM-dependent NF-κB activation and link accelerated aging to a systemic inflammatory response. *Genes Dev*. **26**(20), 2311–2324. PMID: 23019125; doi: 10.1101/gad.197954.112.
65. Keisala T., Minasyan A., Lou Y.-R., … Pyykkö I., Tuohimaa P. (2009). Premature aging in vitamin D receptor mutant mice. *J. Steroid Biochem. Mol. Biol.* **115**(3-5), 91–97. PMID: 19500727; doi: 10.1016/j.jsbmb.2009.03.007.
66. Bouillon R., Carmeliet G., Verlinden L., … Mathieu C., & Demay M. (2008). Vitamin D and human health: Lessons from vitamin D receptor null mice. *Endocr. Rev*. **29**(6), 726–776. PMID: 18694980; doi: 10.1210/er.2008-0004.
67. Richardson P., Griffin I., Tucker C., … Savory E., & Stebbing J. (2020). Baricitinib as potential treatment for 2019-nCoV acute respiratory disease. *The Lancet* **395**(10223), e30–e31. PMID: 32032529; doi: 10.1016/S0140-6736(20)30304-4.
68. Fridman J.S., Scherle P.A., Collins R., … Friedman S.M., & Vaddi K. (2010). Selective inhibition of JAK1 and JAK2 is efficacious in rodent models of arthritis: Preclinical characterization of INCB028050. *J. Immunol.* **184**(9), 5298–5307. PMID: 20363976; doi: 10.4049/jimmunol.0902819.
69. King B., Ohyama M., Kwon O., … DeLozier A.M., & Sinclair R. (2022). Two phase 3 trials of baricitinib for alopecia areata. *New Engl. J. Med.* **386**(18), 1687–1699. PMID: 35334197; doi: 10.1056/NEJMoa2110343.
70. O'Shea J.J., Schwartz D.M., Villarino A.v., Gadina M., McInnes I.B., & Laurence A. (2015). The JAK-STAT pathway: Impact on human disease and therapeutic intervention. *Annu Rev Med.* **66**, 311–328. PMID: 25587654; doi: 10.1146/annurev-med-051113-024537.
71. Hu X., Li J., Fu M., Zhao X., & Wang W. (2021). The JAK/STAT signaling pathway: From bench to clinic. *Signal Transduct. Target Ther.* **6**(1), 402. PMID: 34824210; doi: 10.1038/s41392-021-00791-1.
72. Stolzer I., Dressel A., Chiriac M.T., Neurath M.F., & Günther C. (2021). An IFN-STAT axis augments tissue damage and inflammation in a mouse model of Crohn's disease. *Front Med. (Lausanne)*. **8**, PMID: 34141714; doi: 10.3389/fmed.2021.644244.
73. He C., Medley S.C., Kim J., … Griffin T.M., & Olson L.E. (2017). STAT1 modulates tissue wasting or overgrowth downstream from PDGFRβ. *Genes Dev.*. **31**(16), 1666–1678. PMID: 28924035; doi: 10.1101/gad.300384.117.
74. Huang F., Wang Q., Guo F., … He Y., Qin G. (2019). FoxO1-mediated inhibition of STAT1 alleviates tubulointerstitial fibrosis and tubule apoptosis in diabetic kidney disease. *EBioMedicine* **48**, 491–504. PMID: 31629675; doi: 10.1016/j.ebiom.2019.09.002.
75. van de Veerdonk F.L., Plantinga T.S., Hoischen A., … Veltman J.A., & Netea M.G. (2011). STAT1 mutations in autosomal dominant chronic mucocutaneous candidiasis. *New Engl. J. Med.* **365**(1), 54–61. PMID: 21714643; doi: 10.1056/NEJMoa1100102.
76. Kubben N., Zhang W., Wang L., … Liu G.-H., & Misteli T. (2016). Repression of the antioxidant NRF2 pathway in premature aging. *Cell* **165**(6), 1361–1374. PMID: 27259148; doi: 10.1016/j.cell.2016.05.017.